JOURNAL OF SYNCHROTRON RADIATION
ISSN 1600-5775

Synchrotron-radiation-based X-ray micro-computed tomography reveals dental bur debris under dental composite restorations

Assem Hedayat,[a]* Nicole Nagy,[b] Garnet Packota,[a] Judy Monteith,[a] Darcy Allen,[a] Tomasz Wysokinski[c] and Ning Zhu[c]*

[a]College of Dentistry, University of Saskatchewan, 123-105 Wiggins Road, Saskatoon, Saskatchewan, Canada S7N 5E4, [b]Department of Mechanical and Mechatronics Engineering, University of Waterloo, Ontario, Canada, and [c]Canadian Light Source, Saskatoon, Saskatchewan, Canada. *Correspondence e-mail: assem.hedayat@usask.ca, rickzn@gmail.com

Received 26 October 2015
Accepted 4 February 2016

Edited by A. F. Craievich, University of São Paulo, Brazil

Keywords: in-line phase contrast imaging; micro-computed tomography; dental bur debris; composite resin dental filling; tungsten carbide–cobalt; dentinal tubule; dentinal fluid.

Dental burs are used extensively in dentistry to mechanically prepare tooth structures for restorations (fillings), yet little has been reported on the bur debris left behind in the teeth, and whether it poses potential health risks to patients. Here it is aimed to image dental bur debris under dental fillings, and allude to the potential health hazards that can be caused by this debris when left in direct contact with the biological surroundings, specifically when the debris is made of a non-biocompatible material. Non-destructive micro-computed tomography using the BioMedical Imaging & Therapy facility 05ID-2 beamline at the Canadian Light Source was pursued at 50 keV and at a pixel size of 4 µm to image dental bur fragments under a composite resin dental filling. The bur's cutting edges that produced the fragment were also chemically analyzed. The technique revealed dental bur fragments of different sizes in different locations on the floor of the prepared surface of the teeth and under the filling, which places them in direct contact with the dentinal tubules and the dentinal fluid circulating within them. Dispersive X-ray spectroscopy elemental analysis of the dental bur edges revealed that the fragments are made of tungsten carbide–cobalt, which is bio-incompatible.

1. Introduction

Dental burs can be made of stainless steel, diamond or tungsten carbide (WC) cemented with cobalt or nickel (Ahmed *et al.*, 2014). Tungsten carbide–cobalt (WC-Co) is a bio-incompatible and potentially biohazardous combination of heavy metals (Moulin *et al.*, 1998). Generally, dental burs come in different kinds and shapes. Each of these kinds of burs is used for a specific function when drilling into the crown of a tooth to create a cavity in which filling material is placed. Stainless steel burs are used if the cutting is pursued at speeds slower than 5000 r.p.m., while at high speeds diamond-coated burs are most efficient in carving the brittle enamel, and WC burs are most efficient in cutting dentin (Garg & Garg, 2013). The bur debris can remain within the prepared tooth structure, can also be ingested or inhaled, and, due to their sharp edges, can become lodged in soft tissue. In one study, magnetic resonance (MR) images revealed the presence of dental bur artifacts in both second premolar areas of the mandible. Histological analysis in the same study also revealed bur debris in the gingiva (Kaneda *et al.*, 1998).

The Knoop hardness of the enamel and dentin of natural teeth is reported to be in the range 250–500 kg mm^{-2} and 50–70 kg mm^{-2}, respectively (Braden, 1976; Jackson *et al.*, 2014). The estimated wear rates of a WC-Co dental bur's flank

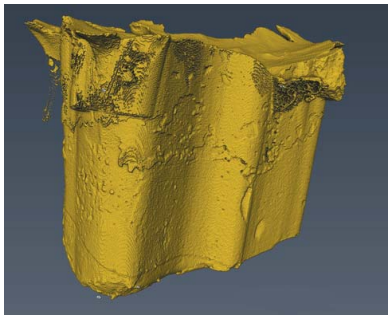

drilling normal teeth are 20, 40, 50, 70 and 75 μm after 30, 90, 210, 330 and 450 s, respectively (Jackson *et al.*, 2014). This indicates that there is substantial debris broken off and released from the dental bur continuously as it carves the tooth. It is uncertain whether the high-speed suction system that is used by dentists during cutting of the teeth using burs can remove all of the dental bur debris from inside the prepared tooth and its biological surrounding.

X-ray micro-computed tomography (μCT) is capable of revealing the three-dimensional microstructure of molars. A conventional μCT with polychromatic beam has been used to visualize the three-dimensional structure of teeth and dental fillings. However, beam-hardening artifacts in μCT of metal objects frequently limit the imaging quality. Because of the energy dependence of the attenuation coefficient, the different energy levels of the polychromatic spectrum are not attenuated in the same manner (Yu *et al.*, 2012). Accordingly, it would be very difficult to study bur debris existing in teeth using this technique. Synchrotron-radiation-based micro-computed tomography (SRμCT) using monochromatic X-ray beam could avoid beam-hardening artifacts. In this study, SRμCT was used to study debris of metallic nature under the composite filling material.

2. Materials and methods

All molars used in this research were extracted teeth that were never previously prepared. After extraction, the teeth were preserved in Carolina solution (Carolina Biological Supply Company, Burlington, NC, USA).

Human molars from the tooth bank at the College of Dentistry, University of Saskatchewan, were used. The molars were prepared using a high-speed hand piece equipped with a new FG 170 high-speed dental bur supplied by Axis Sybron-Endo, Morrisburg, Canada. This is a tapered fissure bur, used to perform cavity preparation in the crowns of these molars (Kaneda *et al.*, 1998).

The occlusal surfaces of the molars were prepared to a minimum depth of about 2.5 mm in the presence of air and water spray to remove debris continuously, and then the prepared surfaces were etched using 3M ESPE Scotchbond™ 35% phosphoric acid etchant gel for 15 s. The etchant was rinsed with water for 15 s, leaving the dentin moist but not wet. A 3M ESPE Adper™ Single Bond Plus adhesive was then applied to the walls and floor of the prepared surface, then carefully air dried for 5 s to evaporate the solvent, then light cured for 20 s with light-emitting diode blue light using SmartLite™, Dentsply, USA. A 3M ESPE Filtek™ Supreme Ultra A3 Body Shade composite restorative material was placed into the cavity preparations in 2 mm increments against the walls and floor of the preparation using a plastic filling instrument. The composite restoration was cured for 20 s per increment using SmartLite™. The 3M ESPE Scotchbond™ etchant, Adper™ Single Bond Plus adhesive, and Filtek™ Supreme Ultra composite resin are all products of 3M, St Paul, USA. The filled molars were then immersed and stored in Carolina solution to avoid drying before imaging. In total, we scanned two molars, restored with dental composite. One restored molar was scanned at the Advanced Light Source, Lawrence Berkeley National Laboratory, beamline 8.3.2, while the other was scanned using beamline 05ID-2 at the BioMedical Imaging & Therapy facility (BMIT) at the Canadian Light Source (CLS). The imaging of the composite restored molars using beamline 8.3.2 at Berkeley and BMIT at the CLS revealed dental bur fragments under the fillings. Since the results are similar, we will summarize the procedure and imaging results achieved at the CLS.

The restored molars were imaged at the 05ID-2 beamline at the CLS (Wysokinski *et al.*, 2015), by means of synchrotron-radiation-based X-ray micro-computed tomography. The imaging was carried out non-destructively, using hard X-rays to provide a high resolution and a sharp phase contrast (Advanced Light Source, 2014). The molars were rinsed with water and dried in air. Each molar was mounted rigidly on a kinematic mount of the sample container within the instrument and centered prior to imaging. The molar was scanned in rotation steps of 180°/3000 and was exposed to a 50 keV X-ray beam for 0.5 s per projection. The projected images were recorded by means of a beam monitor AA-40 (HAMAMATSU) coupled to a charge-coupled device camera (HAMAMATSU C9300-124, 4000 × 2672 pixels) with an effective pixel size of approximately 4.3 μm. Both flat-field corrections (removal of beam-related artifacts) and dark-field corrections (removal of camera-specific artifacts) were applied during reconstruction. Reconstruction of the obtained projections was performed using Gridrec algorithms provided in the software *PITRE 3.1* (Chen *et al.*, 2012). Two-dimensional slices and three-dimensional rendered data were obtained using the software *Avizo 9.0* (FEI, USA) to yield representation of the serial sections. The further segmented components from rendered data representing dental fillings, voids and adhesives, and fragments were used for quantitative analyses including volume and particle sizes.

Two scanning electron microscopes (SEMs) were used to image the dental bur surfaces. The first SEM was a Jeol JSM-6010LV, used to image the surface of the dental burs and measure the pores between the WC-Co particles on their cutting edges. The second SEM was a Jeol JXA-8600 equipped with an energy-dispersive X-ray spectroscope (EDS) to qualitatively analyze the elemental composition of the burs' surface.

3. Results and discussion

3.1. SEM and EDS

Fig. 1(*a*) is a SEM photomicrograph of the cutting edges of an unused dental bur. The surface of the bur has small prominences (arrows) that are approximately 20 μm in size. Fig. 1(*b*) is a magnified micro-image of a part of the cutting edge that delineates the surface morphology of the edge of the unused bur. The particles seen in this image are mainly geometrical in shape, with submicrometer voids in between them. The voids constitute a weakness in the cutting edges of

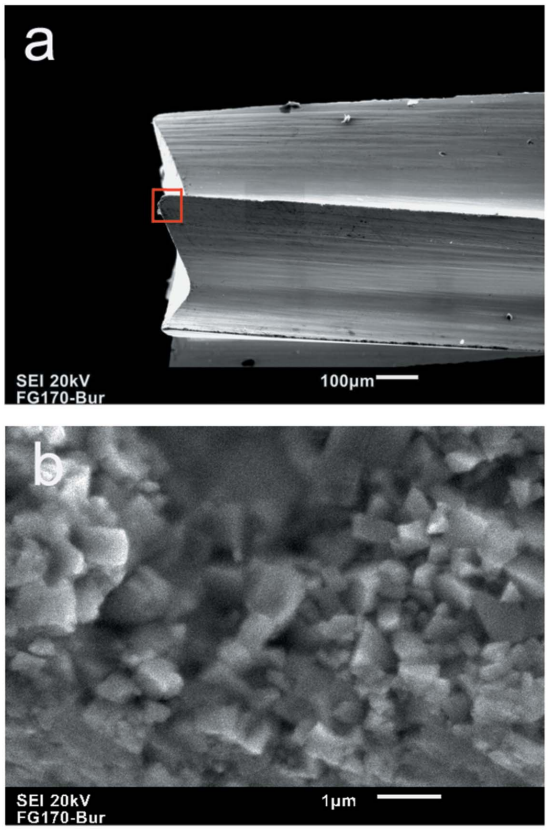

Figure 1
Scanning electron microscopy photomicrographs: (*a*) the tip of an unused WC FG170 dental bur; (*b*) the WC cutting edge of an unused FG170 dental bur which was chosen from the red frame in (*a*); (*c*) energy-dispersive X-ray spectroscopy elemental analysis of the cutting edge of an unused dental bur material.

the bur, making them vulnerable to chipping or fragmenting while cutting calcified tooth structure. Elemental analysis of the dental bur's cutting edge using EDS revealed the presence of a cobalt peak, as shown in Fig. 1(*c*). This means that the dental bur debris is made of WC-Co and not only WC.

3.2. SRμCT

SRμCT revealed shiny debris of metallic nature under the composite filling material. After computed tomography (CT) reconstruction, the data were analyzed to yield image slices of the molars through the sagittal plane of the tooth crown from the lateral surface to the medial surface, as well as in the axial plane from the cusp tips to the base of the crown. These images provided information relevant to whether the debris is directly in contact with the dentin or separated from it by the applied Adper™ Single Bond Plus adhesive. Fig. 2 presents a typical sagittal (side) image of the molar. Not only does it show enamel, dentin and composite restorative filling material, but also Adper™ Single Bond Plus adhesive indicated by arrow A between the filling and dentin. The greyscale at the upper right of Fig. 2 represents the linear attenuation coefficients μ (cm^{-1}), which reflects the density distribution of different materials in the molar. The detected densities for dentin are lower than those of enamel while the detected densities for dental filling material are higher than those of enamel, which is in good agreement with reports in the literature (Weidmann *et al.*, 1967; Coklica *et al.*, 1969). There are also some small areas, such as the areas indicated by arrow B in Fig. 2 inside the fillings with the same density range as those of the air outside the molar, which reflect that there are voids forming during the tooth-filling process. Interestingly, there is an area indicated by arrow C in Fig. 2 between the dentin and filling material showing the linear attenuation coefficient much higher than that of enamel that we believe to be bur fragments. To evaluate the potential of a quantitative material characterization, the linear attenuation coefficient μ has been determined at 14 positions in enamel and 14 positions in fragments. Each region of interest covered $4 \times 4 \times 4$ voxels, which corresponds to a physical size of 5088 μm^3. The results show that the μ values of enamel and fragments at 50 keV are 1.34 (SD: ± 0.05) cm^{-1} and 21.98 (SD: ± 4.28) cm^{-1}, respectively. The measured μ value of the enamel is close to the μ value of compact bone (μ: 1.19 cm^{-1}; density: 2.9 g cm^{-3}) at 50 keV, which was calculated based on the NIST database (http://physics.nist.gov/cgi-bin/Star/compos.pl?refer=ap&matno=119). The linear attenuation coefficient of the bur fragments is over 16 times that of enamel. During the tooth-filling process, the only material

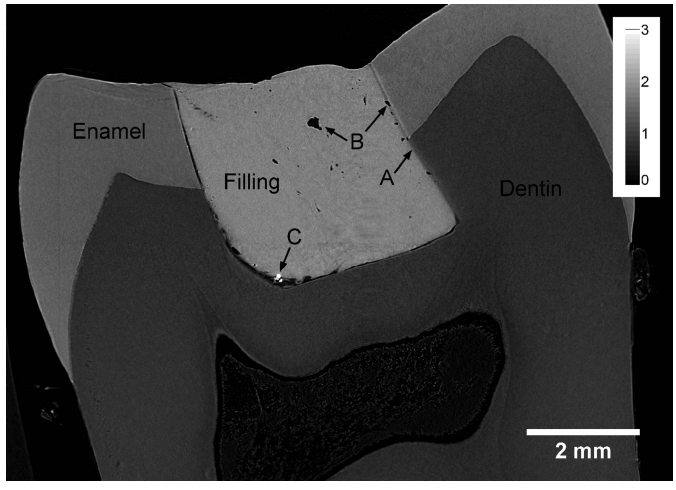

Figure 2
Attenuation-contrast imaging results of a molar with dental composite filling material.

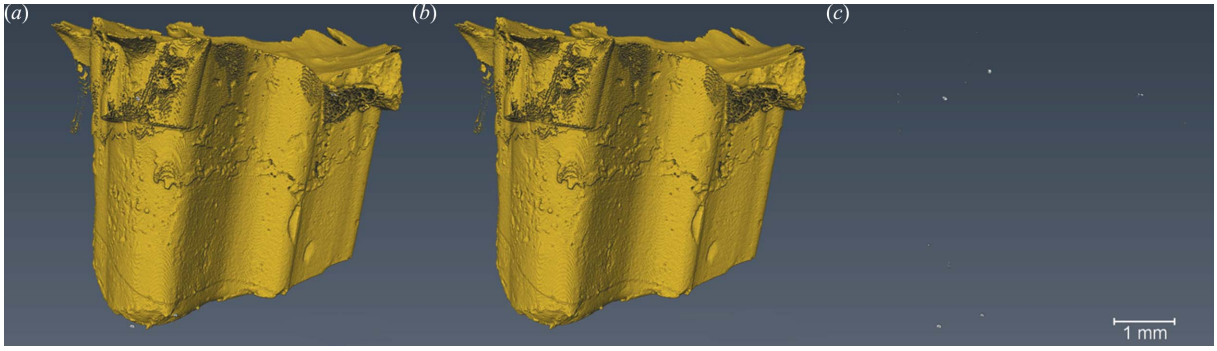

Figure 3
Segmentation results of the molar from volume rendering (*a*) dental composite filling material (yellow) with high density fragments (white); (*b*) dental composite filling material only (yellow); (*c*) high-density fragments only (white).

involved with high density is WC-Co. So the fragments in the images are WC-Co bur debris.

To further quantify the distribution of those fragments, the dental filling material and high-density fragments were segmented from the raw imaging data using *Avizo* (Fig. 3). The volumes of the different components in the molar were calculated based on the segmentation results. The volume of the filling is 33.52 mm^3 and the total volume of the fragments is 6×10^{-4} mm^3. There are 14 fragments in total in the molar. Fig. 4 shows the fragment size distribution. Based on the CT reconstructed results, all the high-density fragments of WC are only found in the space between the tooth and composite restorative fillings. There are no such fragments appearing inside the tooth or fillings. Their diameters are between 19.4 and 74.4 μm and the mean diameter is 34.3 μm. The size of the prominences on the surface of the bur (Fig. 4) is of the same dimensions as the high-density fragments segmented from the CT reconstructed images. It is shown in the SRμCT results that the fragment sizes are between 19.4 and 74.4 μm. The fragments less than 19 μm cannot be detected appropriately due to technical limitations. The physical pixel size of the detector is 4.3 μm. If the fragments are smaller than 4 pixels (∼19 μm) it is difficult to identify them from the image noise. It is possible that there are smaller bur fragments existing in the tooth. During the experiment, we were trying to reduce the effect of phase contrast and the sample-to-detector distance was set at 20 cm to minimize the phase-contrast effects, which is the shortest distance available at the 05ID-2 beamline. The images include both absorption-contrast and some phase-contrast effects. The phase-contrast has an effect on attenuation as not all intensities correspond to changes in density. The phase-contrast depends on the density difference. The sharp phase-contrast appears at the air/enamel interface, but may be significantly reduced at fragments/filling interface. This is because the density difference between air and enamel is an order of magnitude larger than that between fragments and filling. This edge-enhanced phase contrast may also affect the estimates of the small particle sizes and made the calculated volume oversized. This error is minimized at 19 μm and larger. The effect of phase-contrast on the dental filling X-ray images will be investigated in a future study.

In this study, only two molars were restored with composite filling and imaged. Thus, the study is a proof of concept.

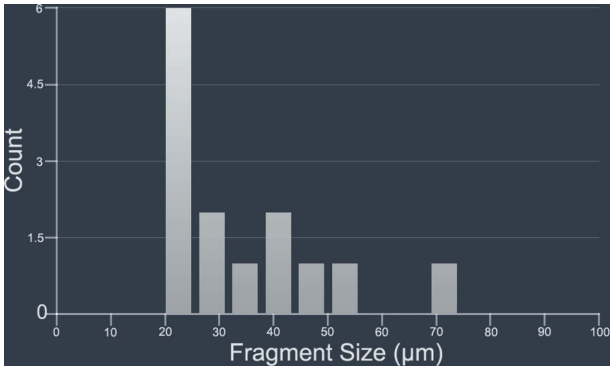

Figure 4
Dental bur fragments size distribution.

3.3. Dentinal tubules and dentinal fluid

Dentinal tubules in humans vary in diameter and density depending on their distance from the pulp. In different regions, the mean diameter varies as follows: close to the pulp, midway between the pulp and the enamel, and at the periphery of the enamel, the dentinal tubules have diameters of 2.5 μm, 1.2 μm and 0.9 μm, respectively. As for the densities of the dentinal tubules, they are 45000 tubules mm^{-2} close to the pulp, 29500 tubules mm^{-2} midway between the pulp and the enamel, and 20000 tubules mm^{-2} at the periphery of the enamel (Garbergolio & Brannstrom, 1976). For decalcified permanent molars, the volume percent of dentinal tubules relative to the overall dentin volume also varies with the distance from the pulp. The tubules' volume percent near the pulp and at the enamel's periphery are 27.7% and 19.1%, respectively (Garbergolio & Brannstrom, 1976; Hoppe & Stuben, 1965). This means that the dentin is more permeable at the pulp. The converging structure of the tubules towards the pulp yields an interesting fluid dynamics process of counter currents; an outward flux of pulpal fluid runs opposite to an inward diffusional flux of bacterial and chemical products. The pressure gradient across the dentin is the driving force of fluid filtration, and fluid filtration is a function of the fourth power of the dentinal tubule's radius (Bouillaguet, 2004; Pashley, 1990).

Dentinal fluid flow within dentinal tubules of molars is affected by the different stages of the filling procedure. The dentinal fluid flows inwards and outwards at different rates depending on the stage. Osmotic, dehydration, thermal and probably mechanical instigation, or combinations of these, affect the magnitude and direction of the dentinal fluid flow. The dentinal fluid flow rates were estimated to be about -1.4 nL s^{-1} cm^{-2} during etching, -11.3 nL s^{-1} cm^{-2} during drying, $+9.8$ nL s^{-1} cm^{-2} during bonding, and $+22.9$ nL s^{-1} cm^{-2} during curing of the dental composite resin (Ratih *et al.*, 2007). Also, the masticatory pressures to which composite resin fillings are subjected generate dentinal fluid movement (Hirata *et al.*, 1991). This fluid and its contents are injected into the pulp in case of intense sympathetic stimulation or vaso-constriction caused by adrenergic drugs (Brown *et al.*, 1969; Pashley, 1997). We hypothesize that the dentinal fluid might reach the dental bur debris that is dispersed on the floor of the sculpted dentin through the severed tubules. We also speculate that any product resulting from the reaction between the dentinal fluid and the dental bur debris is potentially capable of reaching the pulp. Accordingly, more research needs to be pursued to investigate our hypothesis.

3.4. Toxicity of WC-Co

The International Agency for Research on Cancer (IARC) catalogued WC-Co as apparently carcinogenic (Bastian *et al.*, 2009; Moulin *et al.*, 1998), and the US National Toxicology Program proved the carcinogenicity of cobalt (Moulin *et al.*, 1998; National Toxicology Program, 1996). We speculate that the use of WC-Co dental burs to prepare teeth presents a potential biohazard to patients, especially since we have proven in this study that the dental bur debris that might contain cobalt may remain under the restoration in contact with the dentinal fluid. Additional toxicological studies need to be pursued to prove this hypothesis. Bur debris that is scattered or displaced outside the teeth is also of concern, as this debris may be inhaled, ingested or impacted into soft tissues. The debris fragments may have sharp edges conforming to the photomicrograph of the dental bur edge shown in Fig. 1(*b*). The sharp-edged debris is capable of becoming lodged in the gingiva (Kaneda *et al.*, 1998), and there is the potential for the debris to become lodged in soft tissue adjacent to the teeth, and potentially enter the digestive or respiratory systems of the patient. We estimate the combined volume of the dental bur fragments to be 90 μm^3. The permissible exposure limit for cobalt dust is set at 0.02 mg m^{-3} (http://www.dir.ca.gov/title8/5155table_ac1.html).

4. Conclusions

Synchrotron micro-CT data analysis clearly revealed dental bur debris under dental composite restorations. The image results allow for quantification of the bur debris size distribution. Analysis of the images proved that the dental bur debris remains on the floor of the cavity preparation and possibly in direct contact with the dentinal fluid. Elemental analysis of the WC bur used revealed the presence of cobalt in its composition. Tungsten carbide–cobalt is bio-incompatible, and constitutes a potential biohazard for patients.

Acknowledgements

Research described in this paper was performed at the BMIT facility at the Canadian Light Source, which is funded by the Canada Foundation for Innovation, the Natural Sciences and Engineering Research Council of Canada, the National Research Council Canada, the Canadian Institutes of Health Research, the Government of Saskatchewan, Western Economic Diversification Canada, and the University of Saskatchewan. Also, we would like to thank to Dr George Belev, Dr Adam Webb and Denise Miller at BMIT, who make sure the facility is operating for this study. We would also like to express our sincere gratitude to Dr Dula Parkinson at the Advanced Light Source in Berkeley, California, USA for pursuing the initial phase of this research. All human molars used in this research were resourced from the tooth bank at the College of Dentistry, University of Saskatchewan. The teeth were random and not traceable to the patients they were extracted from. Accordingly, it was not necessary to submit a Research Ethics Board application to pursue this research.

References

Advanced Light Source (2014). *Beamline 8.3.2 Manual 2014.* Advanced Light Source, Lawrence Berkeley National Laboratory, Berkeley, CA, USA (retrieved from http://microCT.lbl.gov).
Ahmed, W., Sein, H., Jackson, M. J., Rgo, C., Phoenix, D. A., Elhissy, A. & Crean, S. J. (2014). *Chemical Vapour Deposition of Diamond for Dental Tools and Burs*, 1st ed. New York: Springer.
Bastian, S., Busch, W., Kuhnel, D., Springer, A., Meissner, T., Holke, R., Scholz, S., Iwe, M., Pompe, W., Gelinsky, M., Potthoff, A., Richter, V., Ikonomidou, C. & Schirmer, K. (2009). *Environ. Health Perspect.* **117**, 530–536.
Bouillaguet, S. (2004). *Crit. Rev. Oral. Biol. Med.* **15**, 47–60.
Braden, M. (1976). *Biophysics of the Tooth: Frontiers of Oral Physiology*, 8th ed. London: Academic Press.
Brown, A. C., Barrow, B. L., Gadd, G. N. & Van Hassel, H. (1969). *Arch. Oral Biol.* **14**, 491–502.
Chen, R.-C., Dreossi, D., Mancini, L., Menk, R., Rigon, L., Xiao, T.-Q. & Longo, R. (2012). *J. Synchrotron Rad.* **19**, 836–845.
Coklica, V., Brudevold, F. & Amdur, B. H. (1969). *Arch. Oral Biol.* **14**, 451–460.
Garbergolio, R. & Brannstrom, S. (1976). *Arch. Oral. Biol.* **21**, 355–362.
Garg, N. & Garg, A. (2013). *Textbook of Operative Dentistry*, 2nd ed. New Delhi: Jaypee Brothers Medical Publishers.
Hirata, K., Nakashima, M., Sekine, I., Mukouyama, Y. & Kimura, K. (1991). *J. Dent. Res.* **70**, 975–978.
Hoppe, W. F. & Stuben, J. (1965). *Stoma*, **18**, 38–45.
Jackson, M. J., Sein, H. & Ahmed, W. (2004). *J. Mater. Sci. Mater. Med.* **15**, 1323–1331.
Kaneda, T., Minami, M., Curtin, H. D., Utsunomiya, T., Shirouzu, I., Yamashiro, M., Kiba, H., Yamamoto, H. & Ohba, S. (1998). *Am. J. Neuroradiol.* **19**, 317–319.
Moulin, J. J., Wild, P., Romazini, S., Lasfargues, G., Peltier, A., Bozec, C., Deguerry, P., Pellet, F. & Perdrix, A. (1998). *Am. J. Epidem.* **148**, 241–248.
National Toxicology Program (1996). *Toxicology and carcinogenesis studies of cobalt heptahydrate in F344 rats and B6C3F mice.*

Technical report. NIH publication No. 96–3961. Bethesda: US Department of Health and Human Services.
Pashley, D. H. (1990). *Experimental Endodontics*, edited by L. Spangberg, pp. 19–49. Boca Raton: CRC Press.
Pashley, D. H. (1997). *Crit. Rev. Oral Biol. Med.* **7**, 104–133.
Ratih, D. N., Palamara, J. E. A. & Messer, H. H. (2007). *Dent. Mater.* **23**, 1405–1411.
Weidmann, S. M., Weatherell, J. A. & Hamm, S. M. (1967). *Arch. Oral Biol.* **12**, 85–97.
Wysokinski, T. W., Chapman, D., Adams, G., Renier, M., Suortti, P. & Thomlinson, W. (2015). *Nucl. Instrum. Methods Phys. Res. A*, **775**, 1–4.
Yu, L., Leng, S. & McCollough, C. (2012). *Am. J. Roentgenol.* **199**, S9–S15.